NANO LETTERS

pubs.acs.org/NanoLett

Letter

Reconfigurable Spin-Wave Interferometer at the Nanoscale

Jilei Chen,[▽] Hanchen Wang,[▽] Tobias Hula,[▽] Chuanpu Liu,[▽] Song Liu,[▽] Tao Liu, Hao Jia, Qiuming Song, Chenyang Guo, Yuelin Zhang, Jinxing Zhang, Xiufeng Han, Dapeng Yu, Mingzhong Wu, Helmut Schultheiss, and Haiming Yu*

Cite This: *Nano Lett.* 2021, 21, 6237–6244

Read Online

ACCESS | Metrics & More | Article Recommendations | Supporting Information

ABSTRACT: Spin waves can transfer information free of electron transport and are promising for wave-based computing technologies with low-power consumption as a solution to severe energy losses in modern electronics. Logic circuits based on the spin-wave interference have been proposed for more than a decade, while it has yet been realized at the nanoscale. Here, we demonstrate the interference of spin waves with wavelengths down to 50 nm in a low-damping magnetic insulator. The constructive and destructive interference of spin waves is detected in the frequency domain using propagating spin-wave spectroscopy, which is further confirmed by the Brillouin light scattering. The interference pattern is found to be highly sensitive to the distance between two magnetic nanowires acting as spin-wave emitters. By controlling the magnetic configurations, one can switch the spin-wave interferometer on and off. Our demonstrations are thus key to the realization of spin-wave computing system based on nonvolatile nanomagnets.

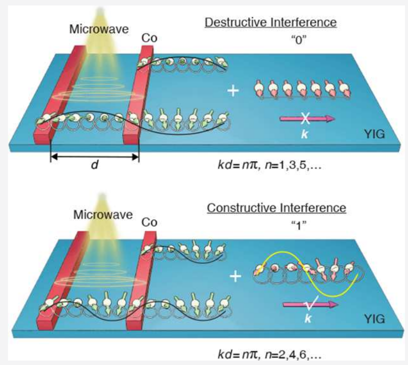

KEYWORDS: *nanomagnonics, spin waves, interferometer, reconfigurability, nanoscale wavelengths*

Spin-based computing systems have recently attracted considerable attentions, given that low-energy consumption, high density, and nonvolatility can be integrated to realize versatile functionalities.[1−5] Magnons, i.e., quanta of spin waves, are promising for the next-generation computing beyond conventional complementary metal oxide semiconductor (CMOS).[6−11] Propagating without charge transport, spin waves are able to transmit information free of joule heating.[12−18] Building spin-wave-based logic architectures with compactness, scalability, and reconfigurability is essential for applications.[19−22] A number of magnonic devices have been successfully demonstrated by using dipolar spin waves with wavelengths above micrometers,[23−25] which are incompatible with high-density integrated circuits.

Interference is crucial for wave-based computing.[26] Spin-wave interference[27−30] allows for designing magnonic logic gates and circuits. So far, interference of spin waves was mainly demonstrated for long-wavelength dipolar spin waves.[29−32] Compared to dipolar spin waves, exchange spin waves[33−40] with short wavelengths and large group velocities are beneficial for building compact and high speed magnonic devices. However, interferometers based on short-wavelength exchange spin waves have not yet been experimentally realized.

In this work, we experimentally demonstrate a nanoscale spin-wave interferometer with a spin-wave wavelength down to 50 nm. Two ferromagnetic nanomagnets serving as short-wavelength magnon emitters are placed with a distance (d) on top of a low-damping magnetic insulator. Interference patterns with constructive and destructive interference are measured in the frequency domain and converted in the wavevector (k) space. The interference pattern is found to be highly sensitive to the variation of d. The spin-wave interferometer is proven to be reconfigurable by switching the double wire system between parallel and antiparallel magnetic configurations. Boolean logics are cascaded based on the spin-wave interferometer as demonstrated by micromagnetic simulations. Our results provide a viable platform for realizing scalable and compact nanomagnonic logic circuits.[41]

■ RESULTS AND DISCUSSION

Figure 1a,b illustrates conceptually the destructive and constructive spin-wave interference realized by two Co nanowires grown on a 20 nm thick YIG film with low magnetic damping.[42−44] A scanning electron microscope (SEM) image of the Co/YIG hybrid structure is shown in Figure 1c, where the width (w) of the Co nanowires is approximately 100 nm and the center-to-center distance (d) between two Co wires is 600 nm. An identical pair of Co nanowires is fabricated 2 μm away as the spin-wave detector. Two nanostriplines with the width of 800 nm are patterned on

Received: May 21, 2021
Revised: July 1, 2021
Published: July 16, 2021

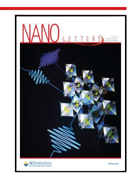

https://doi.org/10.1021/acs.nanolett.1c02010
Nano Lett. 2021, 21, 6237−6244

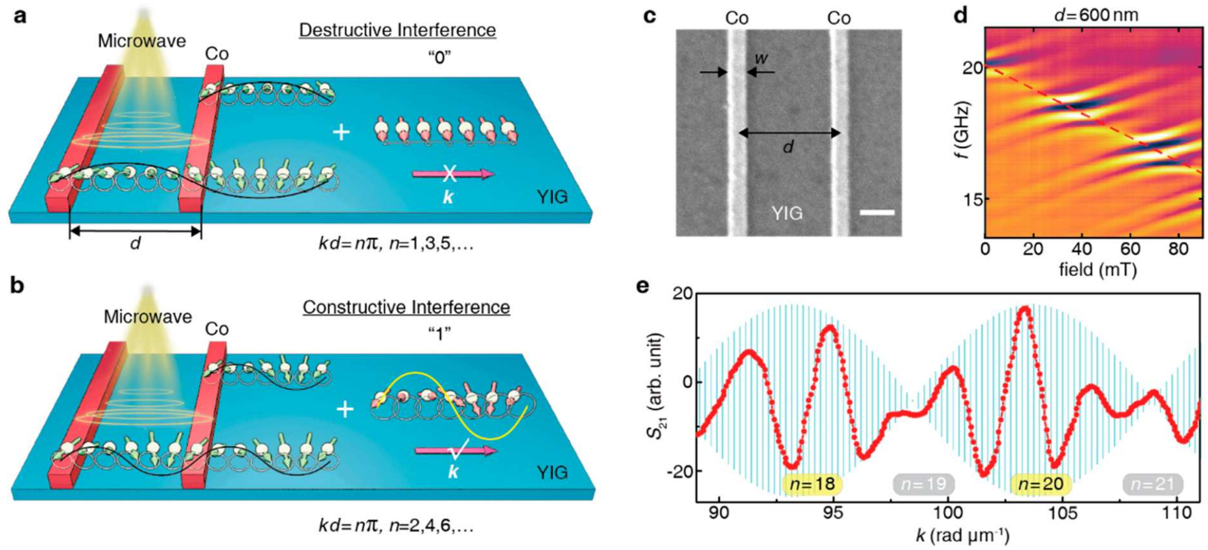

Figure 1. Destructive and constructive interference of spin waves with short wavelengths. (a) Schematic illustration for destructive interference of short-wavelength spin waves in YIG thin films with odd mode numbers, i.e., $kd = n\pi$, n =1, 3, 5, ... The Co nanowires (red bars) are globally excited by a microwave antenna (not shown). (b) Schematic illustration for constructive interference of short-wavelength spin waves in YIG thin films of even mode numbers, i.e., $kd = n\pi$, n =2, 4, 6, ... The spin-wave amplitude is enhanced as shown by the yellow curve. (c) SEM image of a pair of Co nanowires on top of a YIG thin film. The scale bar is 200 nm, the width of Co wires w = 100 nm, and the center-to-center distance of two Co wires d = 600 nm. (d) Microwave transmission spectra measured with a magnetic field applied parallel to the Co wires, where a spin-wave interference pattern in k space is presented after the conversion from frequencies (f) to wavevectors (k) using the calculated dispersions based on ref 48. The red dashed line indicates the FMR mode of Co nanowires. (e) A single transmission spectrum taken along the Co FMR (red dashed line in (d)), where the constructive interference (n = 18 and n = 20) and destructive interference (n = 19 and n = 21) are observed. The light blue bars are wave amplitude packets calculated for the interference pattern based on eq 3 taking an effective distance of 606 nm.

top of those two pairs of Co nanowires. The full range scanning electron microscope (SEM) image of the device structure is shown in the Supporting Information. The ferromagnetic resonance (FMR) of both Co nanowires is uniformly excited by the same microwave stripline antenna, and thus spin waves in YIG films driven by Co nanowires are forced to be coherent. However, the spin waves excited via two Co wires are emitted from different positions, and consequently a phase shift $\Delta\varphi = kd$ is formed between two propagating spin waves, where k stands for the spin-wave wavevector. When the phase shift is $\Delta\varphi = kd = n\pi$ with n being an odd integer, spin waves excited via two Co wires interfere destructively as illustrated in Figure 1a, whereas if the phase shift $\Delta\varphi = kd = n\pi$ with n being an even number, two spin waves interfere constructively and form propagating spin waves with an enhanced amplitude as shown in Figure 1b. The spin-wave interference is experimentally observed by propagating spin-wave spectroscopy (PSWS)[14] measuring the microwave transmission spectra as a function of frequency and magnetic field, as shown in Figure 1d (see Supporting Information Figure S1 for the full spectra). Several strong transmission modes are observed and attributed to the spin waves with even mode numbers, e.g., n = 20. The red dashed line indicates the FMR mode of Co nanowires, whereby the transmission signals are resonantly enhanced[45,46] and also show mode-twisting behaviors in the vicinity of Co resonance (red dashed line in Figure 1d) which may have resulted from a sharp phase shift[47] from Co/YIG magnon coupling. A single spectrum is extracted along the Co FMR mode (the red dashed line in Figure 1d) and shown in Figure 1e as a function of the wavevector k converted from the frequency f according to the dispersions described by ref 48 (see Supporting Information Figure S2). Here, the constructive interference modes n = 18 and n = 20 are enhanced and the signals between constructive interference modes are suppressed and present minima in transmission that are attributed to the destructive interference modes n = 19 and n = 21.

An interference pattern in k space has been demonstrated in Figure 1e with a fixed distance d = 600 nm. We further investigate the spin-wave interference as a function of d between two Co wires serving as spin-wave emitters. The e-beam lithography (see Supporting Information) enables us to reduce the distance down to 200 nm with the Co wire width w ≈ 65 nm as characterized in the SEM image shown as the inset of Figure 2a. The decrease of d will eventually result in an interference pattern with reduced number of periodicity because the propagation phase shift kd would require larger Δk to create a phase change from one constructive interference mode to the next one, e.g., from n = 6 to n = 8 as shown in Figure 2c,e. The observed constructive interference mode n = 8 suggests the excitation and detection of propagating spin waves with a wavelength of λ = 50 nm. If the distance d expands to 1500 nm as shown in Figure 2b, the interference pattern becomes denser in the frequency domain (Figure 2d) and also in k space (Figure 2f) converted from the dispersion relation. The n = 50 mode marked in Figure 2f indicates spin waves with short wavelengths down to 60 nm. Here, another device needs to be fabricated for each distance d. However, if the Co wires are integrated on the recently achieved freestanding positionable microwave antenna,[49] one can sweep the Co wire position and freely tune the spin-wave interference by continuously changing d. The full-range reflection spectra S_{11} and transmission spectra S_{21} measured on the samples with d = 200 nm, d = 600 nm, and d = 1,500 nm are presented in Supporting Information Figure S1. A sketch of the measured device where two nanostripelines are

https://doi.org/10.1021/acs.nanolett.1c02010
Nano Lett. 2021, 21, 6237−6244

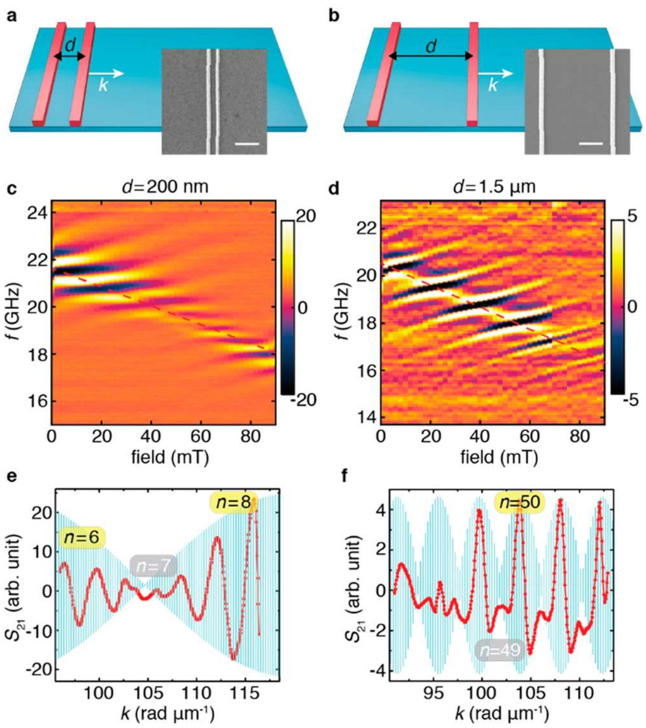

Figure 2. Distance dependence of spin-wave interference. (a) Schematic diagram presenting the device containing two Co wires with distance d = 200 nm. An SEM image is shown in the inset with a scale bar of 500 nm. (b) Schematic diagram presenting the device with d = 1500 nm. The inset shows the SEM image with a scale bar of 500 nm. (c) Microwave transmission spectra S_{21} measured on the device of (a) with d = 200 nm. The magnetic field is applied in parallel to the Co wires. The system is first saturated by a negative saturation field. The field is then swept from 0 to 90 mT with an increment of 2 mT. A single spectrum is extracted along the red dashed line and shown in (e) after the conversion from f to k with the calculated dispersions based on ref 48. A strong spin-wave mode of n = 8 is observed with a short wavelength λ = 50 nm. The light blue bars are wave amplitude packets calculated for the interference pattern based on eq 3 taking an effective distance of 210 nm. (d) Transmission spectra S_{21} measured on the device in (b) with d = 1500 nm. Multiple spin-wave modes are observed, which can also be resolved in the single spectrum extracted along the red dashed line as in (f). The spin-wave mode of n = 50 is marked with a wavelength of 60 nm. The light blue bars are wave amplitude packets calculated for the interference pattern based on eq 3 taking an effective distance of 1512 nm.

integrated on top of each pair of Co nanowires is shown in Supporting Information Figure S7. The magnetization of the YIG film and Co nanowires is initially saturated by a negative field of −120 mT. When the field turns positive, the soft magnetization of YIG is switched, but the magnetization of 100 nm wide Co wires does not switch until the field becomes large enough to overcome their shape-induced anisotropy,[50,51] which results in an antiparallel alignment between Co and YIG magnetization. The spectra in Figure 1e and Figure 2c,d are measured with an antiparallel Co/YIG magnetization alignment where a strong interlayer coupling is formed.[52,53] The anticrossing behaviors of the Co FMR mode and the planar standing wave inside YIG have previously been observed in the studies of the Co/YIG based heterostructures, indicating the existence of the interlayer magnon−magnon coupling. Due to the magnon−magnon coupling, the FMR of Co nanowires can drive exchange spin waves in YIG film. Two beams of spin waves in YIG films excited by two Co nanowires can be used to realize the reconfigurable spin-wave interferometer. The observed strong transmission amplitude was partially from the resonant transducer effect.[45,46] When the Co wires are off resonance, the interference pattern can still be observed but with a lower contrast. The signal oscillations within an individual mode are induced by the spin-wave propagation between excitation and detection antennas. The spin-wave group velocities v_g can be extracted from the observed fringes[14] within one wave packet, which agree well with the k dependent v_g calculated based on Kalinikos and Slavin[48] at low k values but deviate significantly from the theory at high k values. This deviation may be caused by an additional phase shift from the Co/YIG coupling around the Co resonance[47] which contributes to the total phase shift. By taking into account this additional phase shift, the corrected estimation of group velocities agrees with the theory as explained in Supporting Information Figure S3. At destructive interference such as for n = 49 in Figure 2f, the transmission signal is strongly suppressed.

The Object Oriented MicroMagnetic Framework (OOMMF)[54] is exploited to simulate propagating spin waves in YIG films emitted by a pair of Co nanowires with the same dimensions as in the experiments. Figure 3a and Figure 3c show respectively the results of micromagnetic simulations on destructive and constructive spin-wave interference, where the spatial distributions of spin-wave propagation are presented over 1 μm. The detailed parameters used in the simulations are provided in the Supporting Information. The temporal oscillations of the x-component magnetization M_x at x = 1 μm for n = 19 (destructive interference) and n = 20 (constructive interference) are shown respectively in Figure 3b and Figure 3d with approximately 26 times wave amplitude difference. Hence, high-order spin waves (e.g., n = 20) can be efficiently excited and form a strong coherent spin-wave emission due to the constructive interference. Figure 3e shows the simulated spin-wave dispersion with a magnetic field of 50 mT and in an AP configuration. Multiple spin-wave modes can be observed, and their respective excitation efficiency (Figure 3f) can be calculated using fast Fourier transformation (FFT).[55] The micromagnetic simulation results confirm that short-wavelength spin waves with even n can be efficiently emitted but those with odd n are forbidden. An imbalance in magnon population[56] is formed in two individual Co wires at destructive interference[39] revealed by micromagnetic simulations (see Supporting Information Figure S4).

In order to provide an independent evidence for the destructive and constructive spin-wave interference, we utilized Brillouin light scattering microscopy (μBLS) to characterize propagating spin waves in frequency and in space.[15] A sample with 100 nm wide nickel wires and 1.5 μm in period grown on a 20 nm thick YIG thin film is investigated. The measurement protocol is illustrated in Figure 4a, where the spin waves are excited by an integrated stripline antenna covering two Ni nanowires and detected by a focused BLS laser with a spot size of approximately 300 nm in diameter scanning in the x-direction (see Supporting Information for more detailed information). Figure 4b shows the BLS spectra as a function of the applied rf frequency, where a single spectrum is extracted along the diagonal and presented in Figure 4d. The laser spot is located on top of a Ni wire as indicated in Figure 4a with $x \approx 1.5$ μm. Because the BLS setup can only detect

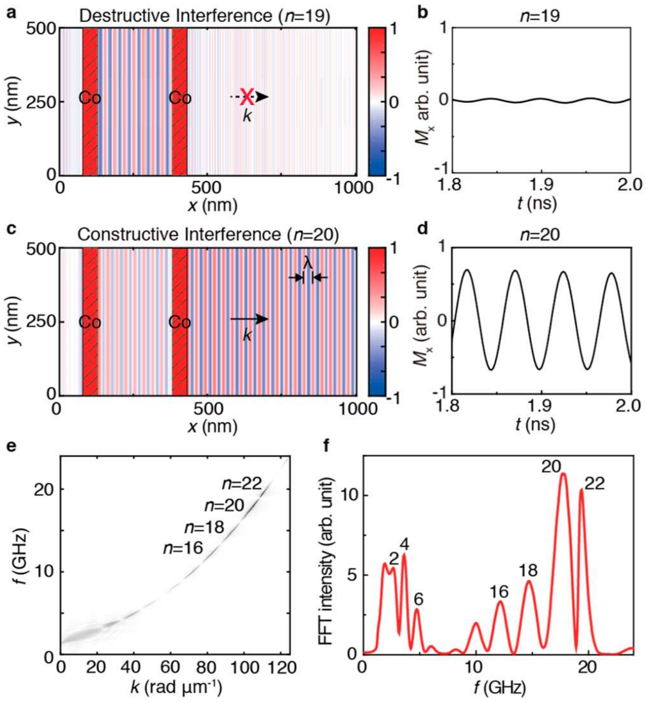

Figure 3. Destructive and constructive spin-wave interference studied by micromagnetic simulations. (a) Spatial map of destructively interfered spin waves with the mode $n = 19$ at 2 ns after the microwave excitation on Co nanowires. The color scale represents normalized spin-wave amplitude in YIG. The red dashed area indicates the Co nanowires. (b) Time-dependent magnetization oscillation (M_x, dynamic component in the x direction is shown) for $n = 19$ mode at $x = 1000$ nm. (c) Spatial map of constructively interfered spin waves with a mode number of $n = 20$ at 2 ns with a short wavelength $\lambda = 60$ nm. The propagating spin waves exhibit large wave amplitude even at $x = 1000$ nm. The temporal oscillation of M_x is shown in (d). (e) Spin-wave dispersion relations derived by micromagnetic simulations using a two-dimensional fast Fourier transformation (FFT). (f) Excitation intensities of various spin-wave modes obtained by one-dimensional FFT.

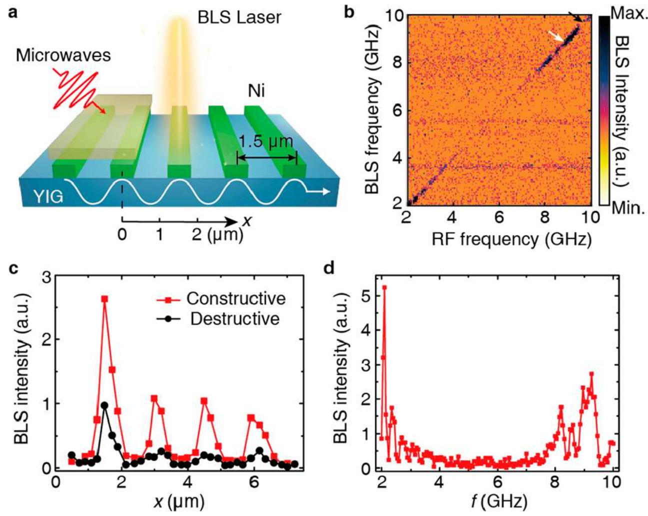

Figure 4. Spin waves detected by microfocused Brillouin light scattering. (a) Illustration introducing the BLS measurement protocol, where spin waves are excited by a stripeline antenna over a pair of Ni nanowire and detected by the BLS laser. The distance between neighboring Ni nanowires is 1.5 μm, and the nanowire width is 100 nm. (b) BLS spectra measured with the BLS laser spot focused on the first Ni wire next to the antenna. The power of the rf excitation on the antenna is set to be 0 dBm. The magnetic hybrid system is initially saturated by a magnetic field of −120 mT and switched to the AP configuration at 27 mT. A single BLS spectrum is extracted along the diagonal and shown in (d). (c) BLS signal intensities measured along the x-direction (as defined in (a)) at 8.8 GHz (red squares) with constructive interference (white arrow in (b)) and 9.7 GHz (black dots) with destructive interference (black arrow in (b)).

spin waves with the wavelength longer than 200 nm due to the diffraction limit,[57] we cannot directly detect exchange spin waves in the YIG thin film. So we focus the BLS laser on Ni nanowires to indirectly detect exchange spin waves due to the dynamic interlayer magnetic coupling between YIG and Ni nanowire. In general, two groups of modes are observed in the vicinity of FMR frequencies of the YIG thin film and Ni wires around 2−4 GHz and 8−10 GHz, respectively. However, in both frequency regions, the spin-wave intensities show several on/off features. The black-color signals indicate strong intensities of spin waves. The spatially resolved BLS measurements are conducted with a laser spot sweeping from $x = 0$ to 7.2 μm (Figure 4a) with an increment of 200 nm. The Ni/YIG bilayer is set to an AP configuration by first applying a negative saturation field of −120 mT and then ramped up to 27 mT in the direction of the Ni wires. The BLS results are shown in Figure 4c for 8.8 and 9.7 GHz as indicated by white and black arrows in Figure 4b, respectively. The first peak of the destructive interference observed in Figure 4c could be due to the far-field directly excited by the antenna. The detected BLS intensity for 8.8 GHz is about 3 times higher on average than that for 9.7 GHz giving evidence for constructive and destructive interference. The full BLS frequency spectra with spatial resolution are shown in Supporting Information Figure S5 for rf excitation frequencies of 8.8 and 9.7 GHz.

When two Co wires are slightly different in width, one wire switches its magnetization earlier than the other during a magnetic field sweep. The sample contains two Co wires on YIG of approximately 190 nm wide for Co(A) and 180 nm for Co(B) with a center-to-center distance $d = 600$ nm. The system is initialized by setting both Co wires in the parallel (P) configuration as shown in Figure 5a with a negative saturation field of −200 mT. The magnetic configurations P state is shown by using magnetic force microscopy (MFM). The same contrast at the end of nanowires indicates that the magnetizations in the neighboring wires are parallel to each other. Figure 5c presents the reflection spectra S_{11} measured with a magnetic field swept from −90 mT to 90 mT. Due to large shape anisotropy, both Co wires stay in the P configuration as shown in Figure 5a until the field is swept to 90 mT (green arrow in Figure 5c) when the wider wire Co(A) switches first and forms an AP configuration as shown in Figure 5b. The bright/dark contrasts at the end of nanowires show the magnetizations in neighboring nanowires are in the antiparallel state. If we fix the applied field at 90 mT and then sweep the field back toward negative values with a decrement of 1 mT, the pair of Co wires remain in the AP configuration from 90 mT down to −90 mT as evidenced by the spin-wave reflection measurement shown in Figure 5d. At each magnetic field, two split Co modes are observed instead of one. With a field applied parallel to Co(A) magnetization (black arrow in Figure 5b), the FMR frequency of Co(A) elevates but that of Co(B) descends as shown in Figure 5d. The reflection spectra shown in Figure 5c and Figure 5d are measured in the same field and

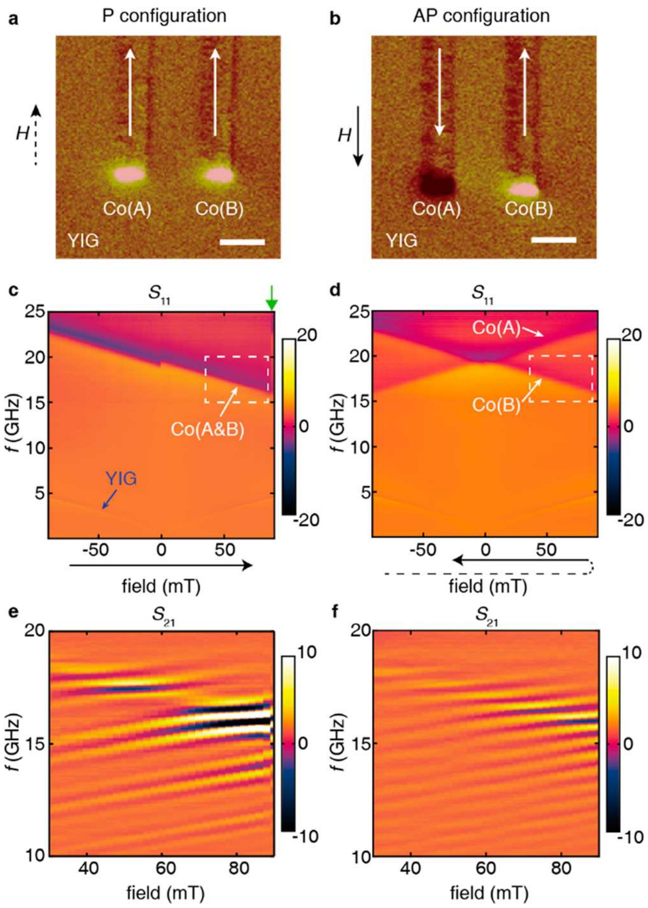

Figure 5. Reconfigurable spin-wave interferometer. (a) MFM image of two Co nanowires grown on the YIG film. The scale bar is 250 nm. A negative saturation field of −200 mT is initially applied along the Co wires as indicated by the black arrow. The white arrows stand for the magnetization orientation of Co(A) and Co(B). Here, a parallel (P) configuration is presented. The antiparallel (AP) configuration is presented in (b). The MFM images are taken at remanent states without bias field. (c) Microwave reflection spectra S_{11} measured on two Co wires with P configuration. The Co and YIG modes are indicated by white and blue arrows, respectively. The magnetic field is swept from negative to positive values. At 90 mT (green arrow), Co(A) starts to switch first due to a slightly larger width than Co(B), and an AP configuration is established. The AP configuration remains when the magnetic field is swept back to negative values as revealed by the measured reflection spectra S_{11} in (d), where two individual Co modes are observed and attributed to Co(A) and Co(B) with opposite magnetization direction as indicated by the white arrows. (e) Microwave transmission spectra S_{21} measured at the P configuration in the frequency and field region marked as the white dashed square in (c). The strongest mode is attributed to constructive interference mode 18π. (f) Transmission spectra S_{21} measured at the AP configuration in the frequency and field region marked in (d) with the magnetic field swept back from high to low values.

frequency range, but because of different field sweeping histories, the results are different. The spin-wave transmission spectra S_{21} are shown in Figure 5e and Figure 5f for the field and frequency range defined by the white dashed squares in Figure 5c and Figure 5d, respectively. When two Co wires are in the P configuration, a clear interference pattern is observed in transmission spectra (Figure 5d) with several spin-wave resonances (e.g., $n = 18$ being the strongest one) consistent with the results in Figure 1d despite different wire widths. However, when two Co wires are switched to the AP configuration, the interference pattern is gone and instead broadband spin-wave transmission spectra is observed with a continuous band of spin waves. This is because only Co(B) is at resonance but Co(A) is off resonance which cannot act as a second spin-wave emitter with comparable amplitude to interfere with spin waves driven by Co(B). As a result, the condition for interference is broken and a broadband spin-wave propagation is formed. Therefore, a reconfigurable spin-wave interferometer is realized with tunable interference by switching the two Co wires between P and AP configurations. Furthermore, this experiment demonstrates a method to read out nonvolatile nanomagnets[58,59] using short-wavelength spin waves at GHz frequencies. Micromagnetic simulations demonstrate the readout of a two-bit magnetic memory using short-wavelength spin waves that are highly sensitive to the P ("0") and AP ("1") configuration of nanomagnets (see Supporting Information Figure S6). On the basis of the recent development of spin-wave nanochannel created by domain walls[15] and nanoconduits,[60,61] the nanoscale spin-wave interferometer studied in this work may be extended to two dimensions or even three dimensions.[62]

In the following, we present a theoretical analysis on spin-wave interference in a double-wire system, where two Co nanowires are globally excited by the microwave stripline. We describe a theorical model for the hybrid system of two Co nanowires whose center is at $\boldsymbol{r}_j = R_j\hat{\boldsymbol{x}}$ ($j = 1, 2$) on YIG, which can be described by a Hamiltonian as

$$\frac{\hat{\mathcal{H}}}{\hbar} = \sum_{j=1,2} \omega^{\mathrm{Co}} \hat{m}_j^\dagger \hat{m}_j + \sum_k \omega_k^{\mathrm{YIG}} \hat{p}_k^\dagger \hat{p}_k + \sum_{j=1,2} \sum_k \left(g_{k,j} e^{-ikR_j} \hat{m}_j \hat{p}_k^\dagger + g_{k,j}^* e^{ikR_j} \hat{m}_j^\dagger \hat{p}_k \right) \quad (1)$$

where $\hat{m}$ and $\hat{p}_k$ are bosonic operators of the Co FMR and spin waves in YIG with wavenumber k, respectively. ω^{Co} and ω_k^{YIG} are resonance frequencies of the Co mode and spin wave modes in YIG. $g_{k,j}(g_{k,j}^*)$ describes the coupling from YIG spin waves (Co FMR) to Co FMR (YIG spin waves). The Kittel mode in two Co wires at R_1 and R_2 are expressed by the operators $\hat{m}_1$ and $\hat{m}_2$, respectively, and the motion equation of the YIG film magnetization reads

$$\frac{d\hat{p}_k(t)}{dt} = -i\omega_k^{\mathrm{YIG}} \hat{p}_k(t) - ig_{k,1} e^{-ikR_1} \hat{m}_1(t) - ig_{k,2} e^{-ikR_2} \hat{m}_2(t) - \frac{\kappa_{\mathrm{YIG}}}{2} \hat{p}_k(t) \quad (2)$$

Here, κ_{YIG} denotes the low intrinsic damping of magnons in the YIG thin films. With the same global driving microwave and high intrinsic damping of Co, we consider the coupling strength g_k and the magnetization dynamics $\hat{m}(t)$ are identical for both Co1 and Co2. Thus, the motion equation of the film magnetization can be simplified as

$$\frac{d\hat{p}_k(t)}{dt} = -i\omega_k^{\mathrm{YIG}} \hat{p}_k(t) - 2ig_k \hat{m}(t) \cos\left(\frac{1}{2}kd\right) e^{-ikR_0} \quad (3)$$

where $d = R_1 - R_2$ is the distance between two Co wires and $R_0 = \frac{1}{2}(R_1 + R_2)$ is the center position of the double-wire system. When $kd = n\pi$ with n being an even number,

https://doi.org/10.1021/acs.nanolett.1c02010
Nano Lett. 2021, 21, 6237−6244

$$\frac{\mathrm{d}\hat{p}_k(t)}{\mathrm{d}t} = -\mathrm{i}\omega_k^{\mathrm{YIG}}\hat{p}_k(t) - 2(-1)^{n/2} ig_k \hat{m}(t)\mathrm{e}^{-ikR_0}$$

resulting in the constructive interference. When $kd = n\pi$ with n being an odd number,

$$\frac{\mathrm{d}\hat{p}_k(t)}{\mathrm{d}t} = -\mathrm{i}\omega_k \hat{p}_k(t)$$

resulting in the destructive interference. According to eq 3, the interference pattern in k space is essentially determined by $\left|\cos\left(\frac{1}{2}kd\right)\right|$, based on which the interference patterns in Figures 1e, 2e, and 2f (light blue bars) are calculated taking effective distances d = 606 nm, 210 nm, and 1,512 nm, respectively, which are in good agreement with the values in the experimental design being d = 600 nm, 200 nm, and 1500 nm. Detailed calculations of the interaction between Co stripes and the underlying YIG film are provided in the Supporting Information.

CONCLUSIONS

In summary, we have demonstrated experimentally the interference of exchange spin waves with wavelength down to 50 nm. With a fixed distance d between two spin-wave emitters, the interference pattern in the frequency domain is observed which can be converted into k space based on the dispersion relation. When the distance d is enlarged or shortened, the oscillating pattern becomes sparser or denser revealing its interference nature. Furthermore, the spin-wave interference can be tuned on and off by switching the magnetic configuration of the pair of ferromagnetic nanowires between parallel and antiparallel, adding the reconfigurability to the interferometer. Finally, the theoretical analysis suggests the magnon−magnon coupling between the ferromagnetic nanowires and the YIG thin film is responsible for the generation of exchange spin waves and their interference. The experimentally demonstrated prototype of a nanoscale spin-wave interferometer can be applied to a great variety of nanomagnets and form crucial building blocks for nanoscale nonvolatile computing at the microwave frequencies.

ASSOCIATED CONTENT

Supporting Information

The Supporting Information is available free of charge at https://pubs.acs.org/doi/10.1021/acs.nanolett.1c02010.

> Reflection and transmission spectra of three devices with 200, 600, and 1500 nm distances between two nanowires, spin-wave dispersion and group velocity of 600 nm distance device, corrected estimation of the spin wave group velocity, imbalanced magnon populations in two Co nanowires, the full BLS frequency spectra with spatial resolution, two-bit magnetic memory based on spin-wave interferometer, calculation of the interaction between Co stripes and the underlying YIG film, optical and SEM images of the device, variation of distance between emitter and detector, detection of the spin-wave interference by a single magnetic nanowire, sample information, and measurement methods (PDF)

AUTHOR INFORMATION

Corresponding Author

Haiming Yu − *Fert Beijing Institute, MIIT Key Laboratory of Spintronics, School of Integrated Circuit Science and Engineering, Beihang University, Beijing 100191, China;* orcid.org/0000-0002-3291-6713; Email: haiming.yu@buaa.edu.cn

Authors

Jilei Chen − *Fert Beijing Institute, MIIT Key Laboratory of Spintronics, School of Integrated Circuit Science and Engineering, Beihang University, Beijing 100191, China; Shenzhen Institute for Quantum Science and Engineering (SIQSE), and Department of Physics, Southern University of Science and Technology (SUSTech), Shenzhen 518055, China;* orcid.org/0000-0001-9619-8514

Hanchen Wang − *Fert Beijing Institute, MIIT Key Laboratory of Spintronics, School of Integrated Circuit Science and Engineering, Beihang University, Beijing 100191, China;* orcid.org/0000-0001-5646-0493

Tobias Hula − *Institute of Ion Beam Physics and Materials Research, Helmholtz-Zentrum Dresden-Rossendorf, Dresden 01328, Germany*

Chuanpu Liu − *Fert Beijing Institute, MIIT Key Laboratory of Spintronics, School of Integrated Circuit Science and Engineering, Beihang University, Beijing 100191, China*

Song Liu − *Shenzhen Institute for Quantum Science and Engineering (SIQSE), and Department of Physics, Southern University of Science and Technology (SUSTech), Shenzhen 518055, China*

Tao Liu − *Department of Physics, Colorado State University, Fort Collins, Colorado 80523, United States*

Hao Jia − *Shenzhen Institute for Quantum Science and Engineering (SIQSE), and Department of Physics, Southern University of Science and Technology (SUSTech), Shenzhen 518055, China*

Qiuming Song − *Shenzhen Institute for Quantum Science and Engineering (SIQSE), and Department of Physics, Southern University of Science and Technology (SUSTech), Shenzhen 518055, China*

Chenyang Guo − *Beijing National Laboratory for Condensed Matter Physics, Institute of Physics, University of Chinese Academy of Sciences, Chinese Academy of Sciences, Beijing 100190, China*

Yuelin Zhang − *Department of Physics, Beijing Normal University, Beijing 100875, China*

Jinxing Zhang − *Department of Physics, Beijing Normal University, Beijing 100875, China;* orcid.org/0000-0001-8977-5678

Xiufeng Han − *Beijing National Laboratory for Condensed Matter Physics, Institute of Physics, University of Chinese Academy of Sciences, Chinese Academy of Sciences, Beijing 100190, China;* orcid.org/0000-0001-8053-793X

Dapeng Yu − *Shenzhen Institute for Quantum Science and Engineering (SIQSE), and Department of Physics, Southern University of Science and Technology (SUSTech), Shenzhen 518055, China*

Mingzhong Wu − *Department of Physics, Colorado State University, Fort Collins, Colorado 80523, United States*

Helmut Schultheiss − *Institute of Ion Beam Physics and Materials Research, Helmholtz-Zentrum Dresden-Rossendorf, Dresden 01328, Germany*

Complete contact information is available at:

https://pubs.acs.org/10.1021/acs.nanolett.1c02010

Author Contributions

$^{\nabla}$J.C., H.W., T.H., C.L., and S.L. contributed equally. H.Y. conceived the experiments and supervised the project. T.L. and M.W. prepared the high-quality YIG films. J.C., H.W., C.L., H.J., Q.S., and C.G. fabricated the nanostructured samples. S.L., X.H., D.Y., and H.Y. supervised the sample preparation. J.C., H.W., C.L., and H.Y. performed the PSWS measurements. T.H. and H.S. performed the BLS measurements. J.C., H.W., T.H., H.S., and H.Y. analyzed the data. J.C. and H.Y. conducted the micromagnetic simulations. J.C., H.W., T.H., H.S., and H.Y. wrote the manuscript. All authors discussed the results and commented on the manuscript.

Notes

The authors declare no competing financial interest.

■ ACKNOWLEDGMENTS

The authors thank M. Madami, G. Gubbiotti, T. Yu, G. E. W. Bauer, L. Flacke, M. Althammer, and M. Weiler for helpful discussions. The authors also acknowledge support from the NSF China under Grants 11674020, 12074026, and U1801661, the 111 Talent Program B16001, the National Key Research and Development Program of China Grants 2016YFA0300802 and 2017YFA0206200. M.W. was supported by the U.S. National Science Foundation (Grant EFMA-1641989).

■ REFERENCES

(1) Romera, M.; et al. Vowel recognition with four coupled spin-torque nano-oscillators. *Nature* **2018**, *563*, 230−234.
(2) Luo, Z.; et al. Current-driven magnetic domain-wall logic. *Nature* **2020**, *579*, 214−218.
(3) Zázvorka, J.; et al. Thermal skyrmion diffusion used in a reshuffler device. *Nat. Nanotechnol.* **2019**, *14*, 658−661.
(4) Zahedinejad, M.; et al. Two-dimensional mutually synchronized spin Hall nano-oscillator arrays for neuromorphic computing. *Nat. Nanotechnol.* **2020**, *15*, 47−52.
(5) Sander, D.; et al. The 2017 Magnetism Roadmap. *J. Phys. D: Appl. Phys.* **2017**, *50*, 363001.
(6) Kruglyak, V. V.; et al. Magnonics. *J. Phys. D: Appl. Phys.* **2010**, *43*, 264001.
(7) Chumak, A. V.; et al. Magnon spintronics. *Nat. Phys.* **2015**, *11*, 453−461.
(8) Neusser, S.; et al. Magnonics: Spin waves on the nanoscale. *Adv. Mater.* **2009**, *21*, 2927.
(9) Lenk, B.; et al. The building blocks of magnonics. *Phys. Rep.* **2011**, *507*, 107−136.
(10) Khitun, A.; et al. Magnonic logic circuits. *J. Phys. D: Appl. Phys.* **2010**, *43*, 264005.
(11) Csaba, G.; et al. Perspectives of using spin waves for computing and signal processing. *Phys. Lett. A* **2017**, *381*, 1471−1476.
(12) Cornelissen, L. J.; et al. Long-distance transport of magnon spin information in a magnetic insulator at room temperature. *Nat. Phys.* **2015**, *11*, 1022−1026.
(13) Demidov, V. E.; et al. Magnetization oscillations and waves driven by pure spin currents. *Phys. Rep.* **2017**, *673*, 1−23.
(14) Vlaminck, V.; et al. Current-induced spin-wave Doppler shift. *Science* **2008**, *322*, 410−413.
(15) Wagner, K.; et al. Magnetic domain walls as reconfigurable spin-wave nanochannels. *Nat. Nanotechnol.* **2016**, *11*, 432−436.
(16) Chang, L.; et al. Spin wave injection and propagation in a magnetic nanochannel from a vortex core. *Nano Lett.* **2020**, *20*, 3140−3146.
(17) Han, J.; et al. Mutual control of coherent spin waves and magnetic domain walls in a magnonic device. *Science* **2019**, *366*, 1121−1125.
(18) Divinskiy, B.; et al. Excitation and amplification of spin waves by spin−orbit torque. *Adv. Mater.* **2018**, *30*, 1802837.
(19) Lan, J.; et al. Spin-wave diode. *Phys. Rev. X* **2015**, *5*, 041049.
(20) Qin, H.; et al. Low-loss YIG-based magnonic crystals with large tunable bandgaps. *Nat. Commun.* **2018**, *9*, 5445.
(21) Haldar, A.; et al. A reconfigurable waveguide for energy-efficient transmission and local manipulation of information in a nanomagnetic device. *Nat. Nanotechnol.* **2016**, *11*, 437−443.
(22) Kostylev, M. P.; et al. Spin-wave logical gates. *Appl. Phys. Lett.* **2005**, *87*, 153501.
(23) Vogt, K.; et al. Realization of a spin-wave multiplexer. *Nat. Commun.* **2014**, *5* (2014), 3727.
(24) Fischer, T.; et al. Experimental prototype of a spin-wave majority gate. *Appl. Phys. Lett.* **2017**, *110*, 152401.
(25) Chumak, A.; et al. Magnon transistor for all-magnon data processing. *Nat. Commun.* **2014**, *5*, 4700.
(26) Podbielski, J.; et al. Spin-wave interference in microscopic rings. *Phys. Rev. Lett.* **2006**, *96*, 167207.
(27) Wang, Q.; et al. Spectrum gaps of spin waves generated by interference in a uniform nanostripe. *Sci. Rep.* **2015**, *4*, 5917.
(28) Perzlmaier, K.; et al. Observation of the propagation and interference of spin waves in ferromagnetic thin films. *Phys. Rev. B: Condens. Matter Mater. Phys.* **2008**, *77*, 054425.
(29) Schneider, T.; et al. Realization of spin-wave logic gates. *Appl. Phys. Lett.* **2008**, *92*, 022505.
(30) Albisetti, E.; et al. Optically inspired nanomagnonics with nonreciprocal spin waves in synthetic antiferromagnets. *Adv. Mater.* **2020**, *32*, 1906439.
(31) Rousseau, O.; et al. Realization of a micrometre-scale spin-wave interferometer. *Sci. Rep.* **2015**, *5*, 9873.
(32) Bertelli, I.; et al. Magnetic resonance imaging of spin-wave transport and interference in a magnetic insulator. *Sci. Adv.* **2020**, *6*, No. eabd3556.
(33) Wintz, S.; et al. Magnetic vortex cores as tunable spin-wave emitters. *Nat. Nanotechnol.* **2016**, *11*, 948−953.
(34) Brächer, T.; et al. Detection of short-waved spin waves in individual microscopic spin-wave waveguides using the inverse spin Hall effect. *Nano Lett.* **2017**, *17*, 7234−7241.
(35) Liu, C.; et al. Long-distance propagation of short-wavelength spin waves. *Nat. Commun.* **2018**, *9*, 738.
(36) Dieterle, G.; et al. Coherent excitation of heterosymmetric spin waves with ultrashort wavelengths. *Phys. Rev. Lett.* **2019**, *122*, 117202.
(37) Chernov, A. I.; et al. All-Dielectric Nanophotonics enables tunable excitation of the exchange spin saves. *Nano Lett.* **2020**, *20*, 5259−5266.
(38) Lee-Wong, E.; et al. Nanoscale detection of magnon excitations with variable wavevectors through a quantum spin sensor. *Nano Lett.* **2020**, *20*, 3284−3290.
(39) Chen, J.; et al. Excitation of unidirectional exchange spin waves by a nanoscale magnetic grating. *Phys. Rev. B: Condens. Matter Mater. Phys.* **2019**, *100*, 104427.
(40) Baumgaertl, K.; et al. Nanoimaging of ultrashort magnon emission by ferromagnetic grating couplers at GHz frequencies. *Nano Lett.* **2020**, *20*, 7281−7286.
(41) Grundler, D.; et al. Spintronics: Nanomagnonics around the corner. *Nat. Nanotechnol.* **2016**, *11*, 407−408.
(42) Liu, T.; et al. Ferromagnetic resonance of sputtered yttrium iron garnet nanometer films. *J. Appl. Phys.* **2014**, *115*, 17A501.
(43) Yu, H.; et al. Magnetic thin-film insulator with ultra-low spin wave damping for coherent nanomagnonics. *Sci. Rep.* **2015**, *4*, 6848.
(44) Papp, A.; et al. Hybrid yttrium iron garnet-ferromagnet structures for spin-wave devices. *J. Appl. Phys.* **2015**, *117*, 17E101.
(45) Au, Y.; et al. Resonant microwave-to-spin-wave transducer. *Appl. Phys. Lett.* **2012**, *100*, 182404.

(46) Yu, H.; et al. Approaching soft X-ray wavelengths in nanomagnet-based microwave technology *Nat. Nat. Commun.* **2016**, *7*, 11255.
(47) Hashimoto, Y.; et al. 180°-phase shift of magnetoelastic waves observed by phase-resolved spin-wave tomography. *Appl. Phys. Lett.* **2018**, *112*, 232403.
(48) Kalinikos, B. A.; et al. Theory of dipole-exchange spin wave spectrum for ferromagnetic films with mixed exchange boundary conditions. *J. Phys. C: Solid State Phys.* **1986**, *19*, 7013−7033.
(49) Hache, T.; et al. Freestanding positionable microwave-antenna device for magneto-optical spectroscopy experiments. *Phys. Rev. Appl.* **2020**, *13*, 054009.
(50) Topp, J.; et al. Making a reconfigurable artificial crystal by ordering bistable magnetic nanowires. *Phys. Rev. Lett.* **2010**, *104*, 207205.
(51) Ding, J.; et al. Magnonic crystal as a medium with tunable disorder on a periodical lattice. *Phys. Rev. Lett.* **2011**, *107*, 047205.
(52) Chen, J.; et al. Strong interlayer magnon-magnon coupling in magnetic metal-insulator hybrid nanostructures. *Phys. Rev. Lett.* **2018**, *120*, 217202.
(53) Li, Y.; et al. Coherent spin pumping in a strongly coupled magnon-magnon hybrid system. *Phys. Rev. Lett.* **2020**, *124*, 117202.
(54) Donahue, M. J.; et al. *OOMMF User's Guide*, version 2.0a2; National Institute of Standards and Technology; http://math.nist.gov/oommf (accessed September 2019).
(55) Wang, Q.; et al. Spin pumping and spin-wave dispersion in nanoscopic ferromagnetic waveguides. *Phys. Rev. Lett.* **2019**, *122*, 247202.
(56) Yu, T.; et al. Magnon trap by chiral spin pumping. *Phys. Rev. B: Condens. Matter Mater. Phys.* **2020**, *102*, 054429.
(57) Madami, M.; et al. Direct observation of a propagating spin wave induced by spin-transfer torque. *Nat. Nanotechnol.* **2011**, *6*, 635−638.
(58) Dutta, S.; et al. Non-volatile clocked spin wave interconnect for beyond-CMOS nanomagnet pipelines. *Sci. Rep.* **2015**, *5*, 09861.
(59) Luo, Z.; et al. Chirally coupled nanomagnets. *Science* **2019**, *363*, 1435−1439.
(60) Heinz, B.; et al. Propagation of spin-wave packets in individual nano-sized yttrium iron garnet magnonic conduits. *Nano Lett.* **2020**, *20*, 4220−4227.
(61) Choudhury, S.; et al. Voltage controlled on-demand magnonic nanochannels. *Sci. Adv.* **2020**, *6*, No. eaba5457.
(62) Gubbiotti, G.; et al. *Three-Dimensional Magnonics: Layered, Micro- and Nanostructures*, 1st ed.; Jenny Stanford Publishing: Delhi, India, 2019; ISBN 9789814800730.

https://doi.org/10.1021/acs.nanolett.1c02010
Nano Lett. 2021, 21, 6237−6244